communications biology

A Nature Portfolio journal

Article

https://doi.org/10.1038/s42003-025-08213-6

NOD1 deficiency promotes inflammation via autophagic degradation of ASK1

Check for updates

Yoshitaka Kimura[1,2] ✉, Miyako Kimura[2,3], Noriko Miura[4], Yusuke Yoshino[1,5] & Hajime Kono[2]

Nucleotide-binding oligomerization domain-containing protein 1 (NOD1) is a pattern recognition receptor of bacterial peptidoglycans. NOD1 facilitates the elimination of invading intracellular bacteria via autophagy induction. Here, we demonstrate that NOD1 exerts an anti-inflammatory effect mediated via the selective autophagy of host cell protein. In our study of *Candida albicans* water-soluble fraction (CAWS)-induced coronary arteritis, which is a mouse model of Kawasaki disease, we observed an exacerbated disease phenotype in NOD1-deficient mice. NOD1 deficiency induced a higher expression of inflammatory cytokines via CAWS and CAWS-induced endoplasmic reticulum (ER) stress in bone marrow-derived dendritic cells. Furthermore, exaggerated inflammation was dependent on apoptosis signal-regulated kinase 1 (ASK1). Notably, NOD1 directly interacted with ASK1, inducing selective autophagy of ASK1, which was dependent on ATG16L1, and thus competitively inhibiting ER stress-dependent ASK1 activation. Altogether, these results show that NOD1 modulates excessive inflammatory responses through the upregulation of autophagy.

Nucleotide-binding domain leucine-rich repeat–containing receptors (NLRs) are intracellular immune receptors found in plants and animals[1]. Nucleotide-binding oligomerization domain-containing protein 1 (NOD1), a prototypical NLR, is a pattern recognition receptor for peptidoglycans in gram-negative bacteria. NOD1 orthologs are found in almost all vertebrates, being highly conserved among mammals[2]. Furthermore, NOD1 is ubiquitously expressed across mouse and human tissue, whereas NOD2 expression, for example, is restricted to immune cells and the intestine[3].

NOD1 recognizes bacteria, interacting with receptor-interacting serine/threonine-protein kinase 2 (RIPK2) to then activate NF-κB-driven inflammatory responses[4]. Bacterial infection- and NOD1 agonist-induced inflammation are suppressed in NOD1-deficient (NOD1-KO) mice. However, various studies on antitumor immunity[5], arthritis[6], and colitis[7] have reported exaggerated inflammatory responses in NOD1-KO mice, suggesting anti-inflammatory effects of NOD1.

Autophagy facilitates the turnover of organelles and cellular macromolecules through degradation. Autophagic substrates are encapsulated in autophagosomes and transported to lysosomes for degradation, ensuring intracellular quality control[8]. Autophagy also plays an essential role in regulating immunity and inflammation. Various microorganisms[9–11] and pathogen-associated molecular patterns (PAMPs)[12] are taken up by cells and degraded through autophagy. Damage to organelles, such as the mitochondria and lysosomes, can induce inflammation. Autophagy degrades damaged organelles, protecting host cells from aberrant inflammation[13,14]. It also regulates inflammatory signaling through the degradation of inflammasomes[15,16] and other inflammation-related factors[17]. Collectively, these roles of autophagy help suppress excessive inflammation, while autophagy impairment induces chronic inflammation and has been implicated in autoimmune[18], metabolic[19], cardiovascular[20], and neurodegenerative diseases[21].

Recently, NOD1 has been associated with autophagy. NOD1 binds to LC3, a major autophagy factor, promoting autophagic flux[22]. NOD1 was also reported as associated with xenophagy, a mechanism for eliminating bacteria through autophagy. NOD1 binds to intracellular bacteria and directs them into autophagolysosomes[23]. However, whether the association of NOD1 with autophagy influences cellular functions other than the elimination of bacteria remains unclear.

Kawasaki disease (KD) is an acute febrile illness and systemic vasculitis in children with coronary arteritis that can be fatal. NOD1 is thought to be involved in the development of coronary arteritis in KD[24]. The NOD1 agonist FK565 induces coronary arteritis similar to KD in mice. One NOD1 variant was previously associated with a lower risk of KD development[25]. Meanwhile, NOD1-activating ligands were not detected in the serum samples from patients with KD[26]. Other PAMPs (*Candida albicans* water-soluble fraction (CAWS)[27] and *Lactobacillus casei* cell wall extract (LCWE)[28]) also induce coronary arteritis, similar to KD. To clarify whether

[1]Department of Microbiology and Immunology, Teikyo University School of Medicine, Tokyo, Japan. [2]Department of Internal Medicine, Teikyo University School of Medicine, Tokyo, Japan. [3]Division of Regenerative Therapy, Graduate School of Medicine, Juntendo University, Tokyo, Japan. [4]Center for the Advancement of Pharmaceutical Education, Tokyo University of Pharmacy and Life Sciences, Hachioji, Japan. [5]Asia International Institute of Infectious Disease Control, Teikyo University, Tokyo, Japan. ✉e-mail: yo.kimura.july@med.teikyo-u.ac.jp

NOD1 is a driver or trigger of the inflammatory response in KD, we sought to induce coronary arteritis in NOD1-KO mice using stimuli other than FK565.

Herein, we constructed a CAWS-induced coronary arteritis NOD1-KO mouse model. Notably, arteritis was exaggerated in NOD1-KO mice. NOD1 was not essential for coronary arteritis development, while NOD1 exhibited protective activity against CAWS-induced inflammation. This anti-inflammatory function of NOD1 was related to autophagy. In fact, NOD1 induced selective autophagy of ASK1, preventing its activation and suppressing inflammation. Overall, we demonstrate that NOD1 deficiency induces excessive inflammation in response to stress, mediated through the dysfunctional autophagy of host cell protein.

Results

CAWS-induced coronary arteritis was exaggerated in NOD1-KO mice

CAWS, an extract of the *Candida albicans* cell wall, is a PAMP that acts as a ligand for the C-type lectin receptor dectin-2[29]. CAWS induces subacute inflammation in the coronary arteries and aortic roots of mice[27]. We administered CAWS to wild-type (WT) and NOD1-KO mice to examine the role of NOD1 in CAWS-induced coronary arteritis (Fig. 1a). Coronary arteritis was induced in both WT and NOD1-KO mice. Panvasculitis was observed in 70% (7/10) of WT mice and 100% (7/7) of NOD1-KO mice (Fig. 1b). However, the number of lesions, severity, and inflamed area were considerably higher in the NOD1-KO mice (Fig. 1c–e). In all NOD1-KO mice, lesions extended throughout the surrounding aortic root, with extensive inflammatory cell infiltration. In contrast, lesions in most WT mice were localized to a part of the aortic root (Fig. 1a). Furthermore, plasma IL-1β and IL-6 levels were increased in NOD1-KO mice with CAWS-induced vasculitis, reflecting inflammation (Fig. 1f, g).

NOD1 deficiency promotes CAWS-induced inflammatory cytokines

CAWS-induced coronary arteritis is dependent on interleukin (IL)-1β[30]. IL-1β production stimulates monocyte- and neutrophil-driven inflammation within lesions. Administration of anti-IL-1β antibody[31] as well as IL-1β or IL-1 receptor genetic deficiency[32,33] remarkably reduce inflammatory cell infiltration into the aortic root, suppressing coronary arteritis development. Indeed, IL-1β production in lesions was increased in NOD1-KO mice with CAWS-induced vasculitis as were plasma IL-1β levels (Fig. 1f and h). To investigate whether exaggerated coronary arteritis in NOD1-KO mice depends on IL-1β, the IL-1 receptor was knocked out, and CAWS was administered to induce coronary arteritis in these NOD1/IL-1R1-double knockout (DKO) mice. CAWS-induced coronary arteritis was completely suppressed in NOD1/IL-1R1-DKO mice (Supplementary Fig. 1). These results indicated that the aggravation of coronary arteritis in NOD1-KO mice depends on IL-1 signaling.

In a mouse model of KD, IL-1β was reportedly produced by CD11c + F4/80+ macrophages or monocyte-derived dendritic cells[30,34]. We also confirmed IL-1β production by F4/80+ cells (Supplementary Fig. 2a).

To investigate the inflammatory response against CAWS under NOD1 deficiency, we used adherent bone marrow (BM)-derived dendritic cells (BMDCs), which were reported to be CD11c + F4/80+[35] and exhibited high reactivity against CAWS (Supplementary Fig. 2b). The expression levels of IL-1β and IL-6 in adherent BMDCs stimulated with CAWS were evaluated. CAWS-induced IL-6 expression was greater in NOD1-KO BMDCs (Fig. 2a, b), whereas the expression of proIL-1β and secretion of IL-1β were not different from those in WT and NOD1-KO BMDCs stimulated with CAWS (Fig. 2c, d).

Within inflammatory lesions, ATP is released from dead cells or from cells exposed to stress, acting as a damage-associated molecular pattern (DAMP)[36–39]. ATP activates the NLRP3 inflammasome, inducing IL-1β maturation and secretion. In coronary arteritis in KD, cell death, such as necrosis and pyroptosis, is observed, with DAMPs released from dead cells playing important roles in the development of arteritis[40,41]. Therefore, the effects of DAMPs produced in the lesion were considered, and BMDCs were stimulated with both CAWS and ATP. Upon stimulation with CAWS and ATP, IL-1β secretion and caspase-1 activation were greater in NOD1-KO BMDCs than in WT BMDCs (Fig. 2d and Supplementary Fig. 3). Prior to CAWS stimulation, there was no difference in NLRP3 protein levels. However, after significantly upregulated NLRP3 in NOD1-KO BMDCs (Fig. 2e). In summary, CAWS stimulation induced higher NLPR3 expression in NOD1-KO BMDCs, and further stimulation with ATP promoted NLRP3 inflammasome activation and IL-1β secretion.

To elucidate the mechanism underlying exacerbated inflammation in CAWS-stimulated NOD1-KO mice, gene expression differences among BMDCs from WT and NOD1-KO mice were evaluated through RNA-sequencing (RNA-seq). Enrichment analysis of differentially expressed genes (DEGs) in CAWS-stimulated BMDCs revealed differential inflammation-related expression. Furthermore, MAPK signaling-associated genes exhibited notable differential expression (Fig. 2f and Supplementary Table 1). Gene set enrichment analysis (GSEA) indicated that MAPK and p38 MAPK signaling gene sets exhibited significant differential expression between CAWS-stimulated WT and NOD1-KO BMDCs (Fig. 2g). Therefore, MAPK cascade activity after CAWS stimulation was examined via a MAPK phosphorylation array to evaluate MAPK and MAPKK activities. Several MAPKs and MAPK kinases (MAPKKs) were more active in NOD1-KO BMDCs (Fig. 2h). This suggested that NOD1 affects a factor further upstream.

CAWS activates the dectin-2 receptor, resulting in the activation of NF-κB and MAPK, which is dependent on CARD9 and Syk[29,42]. Cell surface expression of dectin-2 did not differ among BMDCs from WT and NOD1-KO mice, nor did the expression of *CARD9* and *Syk* (Supplementary Fig. 4a, b). These results indicate that the greater MAPK activation under NOD1 deficiency was mediated via pathways other than the dectin-2–Syk–CARD9 pathway.

CAWS triggers ER stress

CAWS-stimulated signaling was examined to identify the upstream pathway underlying MAPK cascade activation. Inflammation triggered by cytokines, pathogens, or damaged cells can induce ER stress. Inflammation-induced ER stress activates various signaling pathways, including MAPK signaling, to stimulate further inflammation or apoptosis[43]. RNA-seq revealed considerable enrichment of ER stress-related genes among DEGs before and after CAWS stimulation of BMDCs from both WT and NOD1-KO mice (Supplementary Fig. 5a). Furthermore, many ER stress-related genes were associated with MAPK signaling and inflammation (Fig. 3a and Supplementary Table 2). ER stress marker levels (CHOP and splicing of XBP1) were evaluated, increasing after CAWS stimulation in both WT and NOD1-KO mice (Fig. 3b, c). These results demonstrated that CAWS stimulation induces ER stress in BMDCs.

ER stress and CAWS-induced inflammation mediated via ASK1 was regulated by NOD1

Next, we investigated whether there are differences between WT and NOD1-KO mice in their responses to ER stress. After stimulating BMDCs with ER stress inducer thapsigargin, we observed IL-6 and pro-IL-1β upregulation in NOD1-KO BMDCs (Fig. 3d, e and Supplementary Fig. 5b). Similarly, siRNA-induced NOD1 knockdown in WT BMDCs increased cytokine expression (Fig. 3f).

ER stress is sensed by receptors on the ER membrane, such as IRE1α[43]. Addition of KIRA6, an IRE1α inhibitor, attenuated the exaggerated inflammation in NOD1-KO BMDCs (Fig. 3g). ER stress-activated IRE1α induces inflammatory cytokine expression in two ways. One is through its function as an RNase, whereby it splices *XBP1* mRNA, which is then translated to induce inflammatory cytokine expression[44,45]. Inhibition of IRE1α RNase activity by 4μ8C decreased IL-6 expression, but the difference between WT and NOD1-KO cells was not diminished (Supplementary Fig. 5c). Furthermore, *XBP1* mRNA splicing did not differ between WT and NOD1-KO BMDCs (Supplementary Fig. 5d).

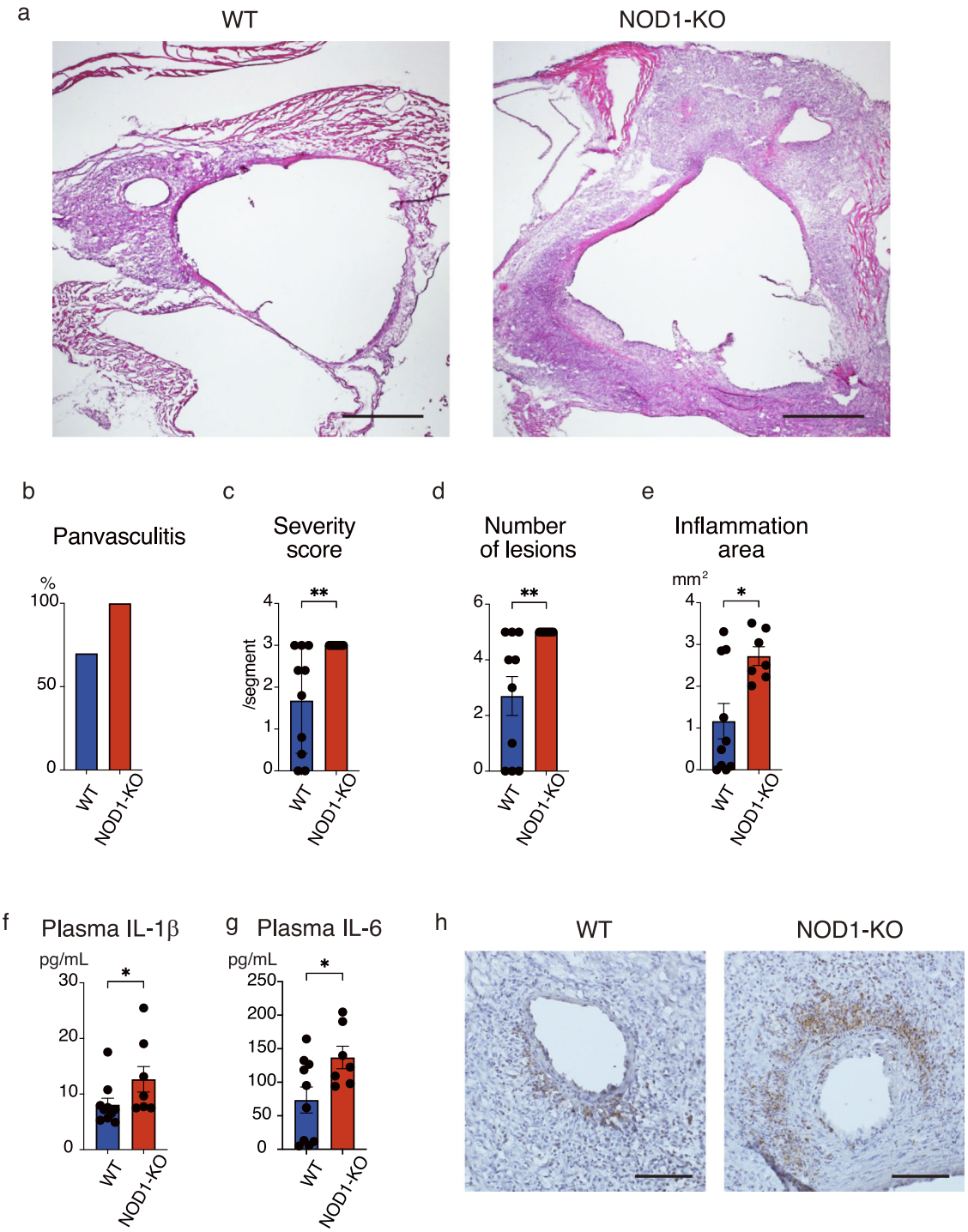

Fig. 1 | NOD1 deficiency aggravates CAWS-induced coronary arteritis. CAWS (2 mg/d) was injected intraperitoneally into WT ($n = 10$) and NOD1-KO ($n = 7$) mice on five consecutive days. At 28 d after CAWS injection, the mice were sacrificed. The degree of inflammatory cell infiltration around the coronary arteries and aortic roots was semi-quantitatively evaluated. Lesions were assessed in the following five segments: left and right coronary arteries, left and right coronary sinuses, and non-coronary sinus. The degree of inflammation in each segment was assessed as follows: 0, no inflammation; 1, inflammation in the intima (endarteritis); 2, inflammation in the intima and adventitia; and 3, inflammation in all layers of the vascular wall (panvasculitis). **a** Hematoxylin–eosin staining of the coronary arteries and the aortic roots. Bars represent 500 μm. **b**–**e**. The severity of coronary arteritis. **b** Prevalence rate of panvasculitis, **c** average severity score per segment in each mouse, **d** number of involved lesions (≥ grade 1) in each mouse, and **e** area of inflammatory cell infiltration in each mouse. **f**, **g** Plasma (**f**) IL-1β and (**g**) IL-6 levels at 28 d in WT and NOD1-KO mice with CAWS-induced coronary arteritis measured via ELISA. **c**–**e**, **g**, **h**: Mann–Whitney *U* test; $^{*}p < 0.05$ and $^{**}p < 0.01$. **h** Immunohistochemistry for IL-1β around the coronary arteries. Bars represent 100 μm. Data represent mean ± SEM. WT wild-type, NOD1-KO NOD1-deficient, CAWS *Candida albicans* water-soluble fraction.

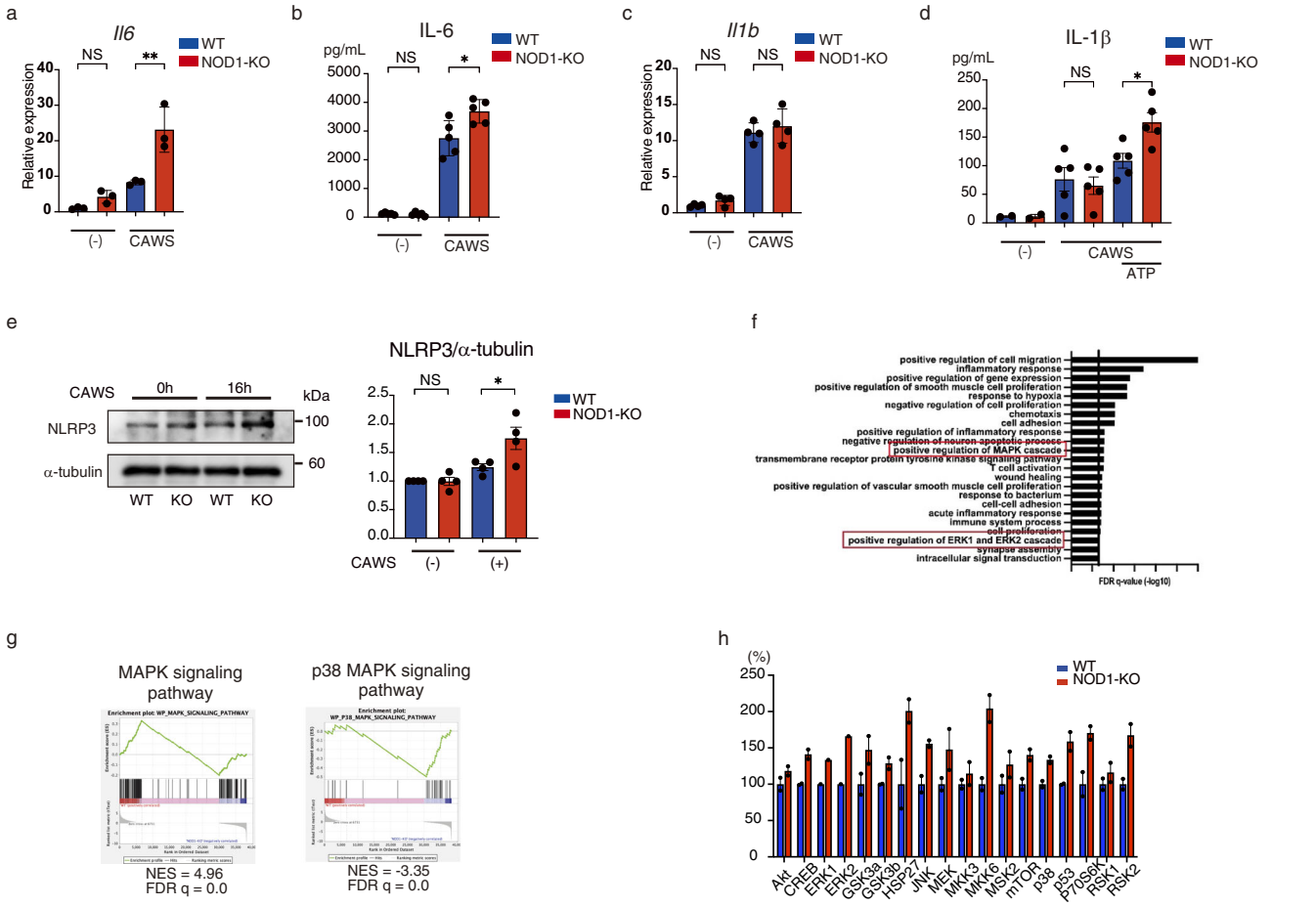

Fig. 2 | NOD1 deficiency promotes CAWS-induced inflammatory cytokine production. a–e Bone marrow-derived dendritic cells (BMDCs) derived from WT and NOD1-KO mice stimulated with CAWS and/or ATP. **a**, **c** Expression of IL-6 (**a**) and IL-1β (**c**) in BMDCs stimulated with CAWS for 24 h measured via RT-PCR. Brown–Forsythe and Welch's ANOVA test with Dunnett's test; $^{**}p < 0.01$ and NS $p > 0.05$. **a** $n = 3$, **c** $n = 4$. **b** IL-6 levels in the supernatant of BMDCs stimulated with 100 μg/mL CAWS for 24 h measured via ELISA. Brown–Forsythe and Welch's ANOVA test with Dunnett's test; $^{*}p < 0.05$ and NS $p > 0.05$. $n = 5$. **d** IL-1β levels in the supernatant of BMDCs stimulated with 100 μg/mL CAWS and/or 1 mmol/L ATP added after 24 h measured via ELISA. Brown–Forsythe and Welch's analysis of variance (ANOVA) test with Dunnett's test; $^{*}p < 0.05$ and NS $p > 0.05$. (−) $n = 2$, (CAWS, CAWS + ATP) $n = 5$. **e** NLRP3 protein levels after CAWS stimulation. Repeated measures one-way ANOVA test with Dunnett's test; $^{*}p < 0.05$, and NS $p > 0.05$. $n = 4$. **f–h** Gene expression analysis via RNA-seq and a phosphorylation array of MAPK proteins in CAWS-stimulated BMDCs. **f** Enrichment analysis of GO biological processes (BP). **g** Gene set enrichment analysis. **h** A phosphorylation array of MAPK proteins in CAWS-stimulated BMDCs. $n = 1$ or 2. Data represent mean ± SEM. WT wild-type, NOD1-KO NOD1-deficient, CAWS *Candida albicans* water-soluble fraction, NS not significant, FDR false discovery rate, GO Gene Ontology, NES normalized enrichment score, POS positive control, NEG negative control.

This suggested that IRE1α RNase activity was responsible for ER stress-induced cytokine production but was not involved in exaggerated inflammation under NOD1 deficiency. Next, we evaluated the contribution of IRE1α protein kinase activity. Activated IRE1α forms a complex with TRAF2 and ASK1[46]. Subsequently, IRE1α directly phosphorylates ASK1, activating the MAPK pathway and inducing inflammatory responses[43]. The IRE1α–ASK1–MAPK pathway was inhibited by ASK1 inhibitor selonsertib, which suppressed IL-6 expression changes in NOD1-KO BMDCs (Fig. 3h). These results were similar to those obtained for pro-IL-1β (Supplementary Fig. 5e–g).

Next, we investigated ASK1 and MAPK pathway activity. The protein levels of ASK1 and ER stress-induced ASK1 phosphorylation increased in NOD1-KO BMDCs (Fig. 3i, j). Additionally, p38 MAPK phosphorylation downstream of ASK1 was greater in NOD1-KO cells compared to that in WT cells (Fig. 3k). These results show that exaggerated inflammation in NOD1-KO BMDCs depends on the IRE1α–ASK1–MAPK pathway. ER stress markers other than MAPK pathway activation were not different between WT and NOD-KO BMDCs (Supplementary Fig. 5d), suggesting that these were not affected by NOD1.

We examined whether ASK1 and MAPK signaling are responsible for the exaggerated CAWS-induced inflammation under NOD1 deficiency. ASK1 inhibitor GS-444217 suppressed the increase in IL-1β and IL-6 levels in NOD1-KO cells stimulated with CAWS and/or ATP (Fig. 3l, m). Furthermore, the increase in NLRP3 expression level under NOD1-KO was also diminished via ASK1 inhibitor treatment (Supplementary Fig. 5h). Adezmapimod, a p38 MAPK inhibitor, also suppressed the increase in IL-1β in NOD1-KO cells (Fig. 3n). These results indicated that the exaggerated inflammation induced by CAWS in NOD1-KO BMDCs is ASK1-p38 MAPK-dependent.

NOD1 induces autophagic degradation of ASK1

Next, we investigated the effect of NOD1 on the IRE1α–ASK1–MAPK pathway. ASK1, TRAF2, and IRE1α were overexpressed, with or without NOD1, in HEK293T cells, to evaluate whether NOD1 is implicated in IRE1α–TRAF2–ASK1 complex formation. Notably, ASK1 protein levels decreased in NOD1-transfected cells, whereas those of other proteins did not (Fig. 4a). ASK1 protein levels were dependent on and inversely related to NOD1 levels. Meanwhile, *ASK1* mRNA levels remained unchanged (Fig. 4b). These results corresponded to changes in NOD1-KO BMDCs,

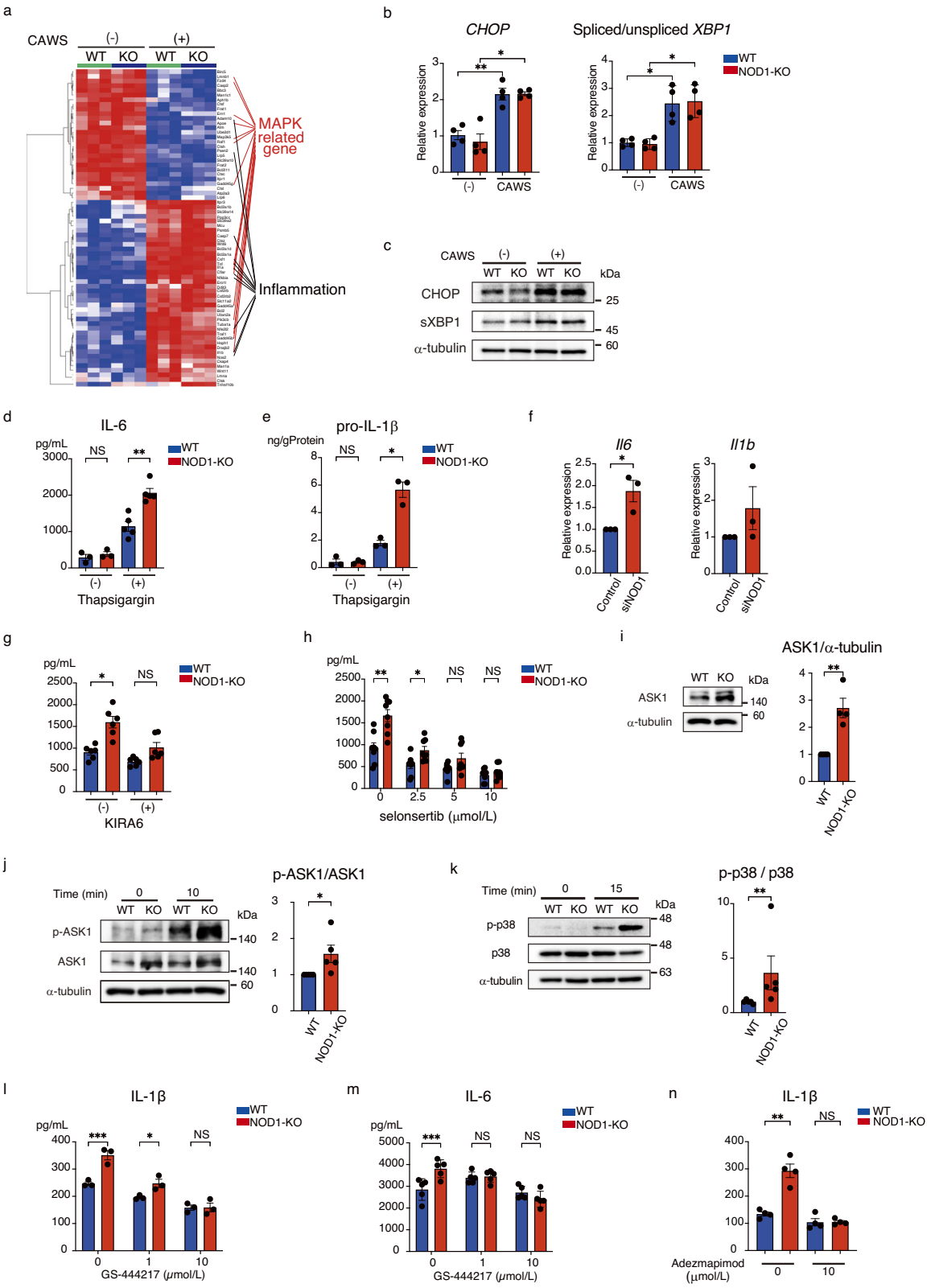

where ASK1 protein levels increased, while *ASK1* mRNA levels did not change (Fig. 3i and Supplementary Fig. 6a).

Thus, we hypothesized that NOD1 affects ASK1 degradation. Protein degradation is mediated via the ubiquitin–proteasome and autophagy pathways. Treatment with proteasome inhibitor MG132 reduced ASK1 protein levels in the presence of NOD1 (Supplementary Fig. 6b). Next, autophagy-mediated degradation investigated using autophagy inhibitors hydroxychloroquine (HCQ), and pepstatin A with E64d. These inhibitors suppressed the decrease in ASK1 expression (Fig. 4c and Supplementary Fig. 6c).

Stable cell lines expressing mCherry-fused ASK1 and EGFP-fused LC3 were generated to investigate ASK1 uptake into autophagosomes. NOD1

Fig. 3 | ER stress- and CAWS-induced inflammation was exaggerated in NOD1-KO mice via the ASK1–MAPK pathway. a Expression of ER-stress-related genes that are differentially expressed in BMDCs before and after CAWS stimulation in RNA-seq. **b**, **c** Expression of ER stress markers in BMDCs stimulated with CAWS was evaluated using (**b**) RT-PCR and (**c**) western blotting. **b** Brown–Forsythe and Welch's analysis of variance (ANOVA) test with Dunnett's test; $^{*}p < 0.05$, and $^{**}p < 0.01$. $n = 4$. **d** IL-6 in the supernatant and (**e**) pro-IL-1β in the cell lysates of BMDCs stimulated with 2 μmol/L thapsigargin for 24 h measured via ELISA. Brown–Forsythe and Welch's ANOVA test with Dunnett's test; $^{*}p < 0.05$, $^{**}p < 0.01$, and NS $p > 0.05$. **d** $n = 3$ or 5, **e** $n = 3$. **f** Expression of IL-6 and IL-1β at 4 h after thapsigargin stimulation of BMDCs with small interfering RNA-induced NOD1 knockdown measured via RT-PCR. Ratio paired-*t* test; $^{*}p < 0.05$. $n = 3$. **g**, **h** IL-6 levels in the supernatant of BMDCs stimulated with thapsigargin for 24 h and/or treatment with (**g**) IRE1α inhibitor KIRA6 or (**h**) ASK1 inhibitor selonsertib measured via ELISA. Brown–Forsythe and Welch's ANOVA test with Dunnett's test; $^{*}p < 0.05$, $^{**}p < 0.01$, and NS $p > 0.05$. **g** $n = 6$, (**h**) $n = 8$. **i**–**k** The ASK1–MAPK pathway activity in thapsigargin-stimulated BMDCs. **i** ASK1 protein levels in BMDCs. Ratio paired-*t* test; $^{*}p < 0.05$. $n = 4$. **j** Phosphorylation of ASK1 of BMDCs after stimulation with thapsigargin (right) and at 10 min after the stimulation (left). Ratio paired-*t* test; $^{*}p < 0.05$. $n = 5$. **k** Phosphorylation of p38 MAPK in BMDCs at 15 min after thapsigargin stimulation. Mann–Whitney *U* test; $^{**}p < 0.01$. $n = 5$. **l**, **n** IL-1β and **m** IL-6 levels in the supernatant of BMDCs stimulated with (**l**, **n**) CAWS and ATP or (**m**) CAWS with the addition of (**l**, **m**) ASK1 inhibitor GS-444217 or (**n**) p38 inhibitor adezmapimod measured via ELISA. **l**, **m** One-way ANOVA with Šídák multiple comparison test; $^{*}p < 0.05$, $^{***}p < 0.001$, and NS $p > 0.05$. **l** $n = 3$, **m** $n = 5$. **n** Brown–Forsythe and Welch's ANOVA test with Dunnett's test; $^{**}p < 0.01$ and NS $p > 0.05$. $n = 4$. Data represent mean ± SEM. WT wild-type, NOD1-KO NOD1-deficient, CAWS *Candida albicans* water-soluble fraction, NS not significant.

overexpression induced the accumulation of ASK1 in autophagosomes (Fig. 4d). These results indicated that NOD1 induces ASK1 degradation via autophagy.

We investigated whether NOD1 increased autophagic flux throughout the cell by assessing LC3 conversion (LC3-I to LC3-II). NOD1 overexpression did not significantly increase LC3 conversion (Supplementary Fig. 7a). Furthermore, the degree of LC3 conversion did not differ between WT and NOD1-KO BMDCs (Supplementary Fig. 7b). These results indicate that NOD1 did not increase non-specific autophagy flux.

Direct interaction of NOD1 with ASK1 induces ATG16L1-dependent autophagy

Next, we aimed to identify the mechanism through which NOD1 induces autophagic degradation of ASK1. Thus, we assessed the NOD1-ASK1 interaction. Hemagglutinin (HA)-tagged ASK1 and FLAG-tagged NOD1 were transfected, and anti-FLAG antibodies were used for immunoprecipitation. NOD1 co-immunoprecipitated with ASK1 (Fig. 5a). Furthermore, when EGFP-NOD1 was transfected into the cell line stably expressing mCherry-ASK1, co-localization was observed (Fig. 5b). These results indicated the direct interaction of NOD1 and ASK1. NOD1 is composed of a leucine-rich repeat (LRR), NACHT, and caspase recruitment domain (CARD). ASK1 co-immunoprecipitated with the LRR and NACHT domains (Fig. 5c). However, transfection with each domain alone did not affect the autophagosomal uptake of ASK1 (Fig. 5d). Next, we hypothesized that autophagy induction requires multiple domains. NOD1 deletion mutants were expressed, with the results showing that LRR or NACHT domain deletion reduced ASK1 autophagy, whereas CARD deletion induced ASK1 uptake into autophagosomes (Fig. 5e, f). The CARD domain, which did not directly bind to ASK1, was not involved in autophagic ASK1 degradation. These results suggest that the interaction between NOD1 and ASK1 is associated with the induction of autophagy against ASK1.

Furthermore, we investigated the interaction of autophagy-related proteins with the NOD1-ASK1 complex. Co-expression of ASK1 and NOD1 and immunoprecipitation with ASK1 resulted in the precipitation of NOD1 and autophagy-related proteins p62 and ATG16L1 (Fig. 6a). p62 functions as a cargo receptor that directs proteins to autophagosomes for selective autophagy[47], and may be involved in ASK1 degradation as such.

ATG16L1 is a key player with important functions at various stages of the autophagic cascade[48]. Reportedly, the NOD1–ATG16L1 interaction is crucial for xenophagy, an autophagic protective mechanism against infection[23]. NOD1 recognizes invasive bacteria, recruiting ATG16L1 and the autophagosome, which wraps around bacteria. To investigate ATG16L1 involvement in the ASK1 degradation process, we generated ATG16L1 knockout cells using the CRISPR/ Cas9 system. The NOD1-induced decrease in ASK1 expression was suppressed in ATG16L1 knockout cells (Fig. 6b). Furthermore, NOD1 protein levels were increased in HCQ-treated cells and ATG16L1 knockout cells, as were ASK1 levels (Figs. 4c and 6d). These results suggested that NOD1 may be degraded together with ASK1. In some cases, NOD1-related autophagy was dependent on RIPK2[49]. However, RIPK2-knockdown did not affect ASK1 degradation by NOD1 (Supplementary Fig. 7c). Collectively, these results indicate that ASK1 is selectively degraded via NOD1-associated autophagy mediated via ATG16L1.

Additionally, we investigated whether the direct interaction between NOD1 and ASK1 affected IRE1α–TRAF2–ASK1 complex formation. In WT cells, it is not possible to compare whether complex formation is competitively inhibited by NOD1, as ASK1 protein levels are altered via NOD1 transfection. Therefore, we used ATG16L1 knockout cells, in which ASK1 was not downregulated. ASK1, IRE1α, and TRAF2 were transfected into cells. Thapsigargin-induced ER stress promoted IRE1α–TRAF2–ASK1 complex formation, resulting in the co-precipitation of IRE1α and ASK1. In contrast, NOD1 transfection decreased the co-precipitation of IRE1α via ASK1 after ER stress induction (Fig. 6c). These results indicate that NOD1 competitively inhibits IRE1α–TRAF2–ASK1 complex formation. The competitive inhibitory effect of NOD1 could explain why ASK1 phosphorylation after ER stress induction increased in NOD1-KO BMDCs (Fig. 3j).

Exaggerated inflammation in NOD1-KO mice with CAWS-induced coronary arteritis was dependent on ASK1

Next, we sought to validate our results in vivo. Notably, ASK1 protein levels were higher in leukocytes from NOD1-KO mice than in those from WT mice (Fig. 7a). We examined the ASK1 dependency of exaggerated inflammation in NOD1-KO with CAWS-induced coronary arteritis. CAWS vasculitis inflamed areas were larger in NOD1-KO sham mice than in WT sham mice. The exaggerated inflammation was reduced via administration of the ASK1 inhibitor selonsertib in NOD1-KO mice (Fig. 7b, c and Supplementary Fig. 8). Moreover, selonsertib reduced plasma IL-1β levels and IL-1β production in the lesions of NOD1-KO mice (Fig. 7d, e). In contrast, inflammation area and coronary arteritis severity in WT mice were not different between those treated with and without selonsertib (Fig. 7b, c). These results demonstrate that the regulation of ASK1 activity by NOD1 is important for suppressing excessive inflammation.

Discussion

In this study CAWS-induced coronary arteritis was exaggerated in NOD1-KO mice. CAWS, LCWE, and FK565, have been reported to induce coronary arteritis through the engagement of innate immunity receptors[24,27,28]. CAWS and LCWE are miscellaneous products extracted from pathogens, inducing coronary arteritis via dectin-2 and Toll-like receptor 2, respectively[42,50]. FK565 is a small-molecule compound that acts as a NOD1 agonist. Our results indicate that NOD1 is not essential for coronary arteritis development but is one of several innate immune receptors involved in its pathogenesis. Evaluating the common pathways acting downstream of these innate immune receptors may be important for elucidating the molecular mechanisms of coronary arteritis development.

NOD1 deficiency promotes CAWS-induced IL-1β secretion and inflammation. Previous studies have shown that NOD1 has anti-

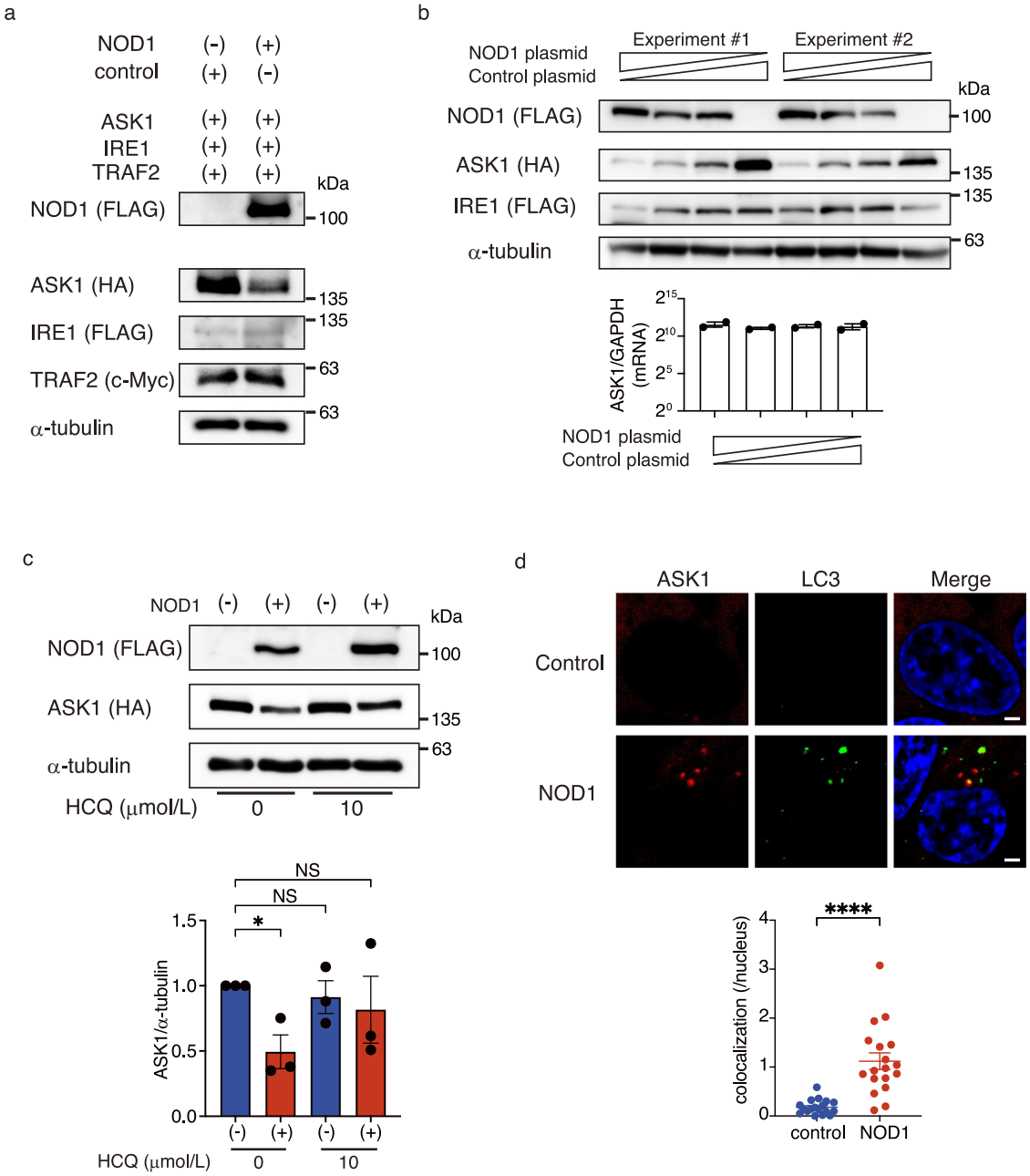

Fig. 4 | NOD1 induces autophagic degradation of ASK1. a Immunoblotting of overexpressed HA-ASK1, FLAG-IRE1α, cMyc-TRAF2, and/or FLAG-NOD1 in HEK293T cells. **b** HEK293T cells overexpressing ASK1 and IRE1α transfected with varying amounts of NOD1. (Upper) Protein levels of each component, and (lower) mRNA expression of ASK1 ($n = 2$). **c** NOD1-induced decrease in ASK1 suppressed by the autophagy inhibitor HCQ. Repeated measures one-way ANOVA test with Dunnett's test; $^{*}p < 0.05$ and NS $p > 0.05$. $n = 3$. **d** NOD1 transfected into a stable mCherry-fused ASK1 (red) and EGFP-fused LC3 (green) cell line. The nucleus was stained with Hoechst33342 (blue). Representative images: bars represent 2 μm. (Graph) Number of colocalized light spots of ASK1 and LC3 per nucleus. Unpaired t-test with Welch's correction; $^{****}p < 0.0001$. $n = 18$. Data represent mean ± SEM. HA hemagglutinin, HCQ hydroxychloroquine, NS not significant.

inflammatory effects, which is in agreement with our findings. *Streptococcus pyogenes* cell wall fragment-induced arthritis was exacerbated in NOD1-KO mice but suppressed in NOD2-KO mice, with enhanced IL-1β expression noted in the swollen joints of NOD1-KO mice[6]. In a colon tumor model, NOD1 suppressed tumor immunity by stimulating the expansion of myeloid-derived suppressor cells. In the same study, NOD1 activation promoted an autophagy-dependent reprograming of macrophages toward an alternative phenotype[5].

Plasma IL-1β levels increased in NOD1-KO mice with CAWS-induced coronary arteritis. In vitro, a difference in IL-1β secretion was only observed in cells stimulated with both CAWS and ATP. This was attributed to differences in NLRP3 expression after CAWS stimulation. The secretion of IL-1β requires two signals: signal 1, which induces the production of pro-IL-1β, and signal 2, which activates the inflammasome to mature IL-1β. However, in vivo each of these stimuli can trigger IL-1β secretion. Intraperitoneal injection of the TLR2 agonist zymosan, which does not activate the inflammasome, induced peritonitis with plasma IL-1β elevation[51]. In contrast, monosodium urate crystals, which are activators of the NLRP3 inflammasome, upregulated IL-1β and IL-1β-dependent inflammatory responses[52,53]. These in vivo results are thought to be related to other PAMPs or endogenous DAMPs released following inflammation or cell death. In the present study, the difference between in vivo and in vitro experiments highlighted the importance of potential DAMPs within inflammatory lesions.

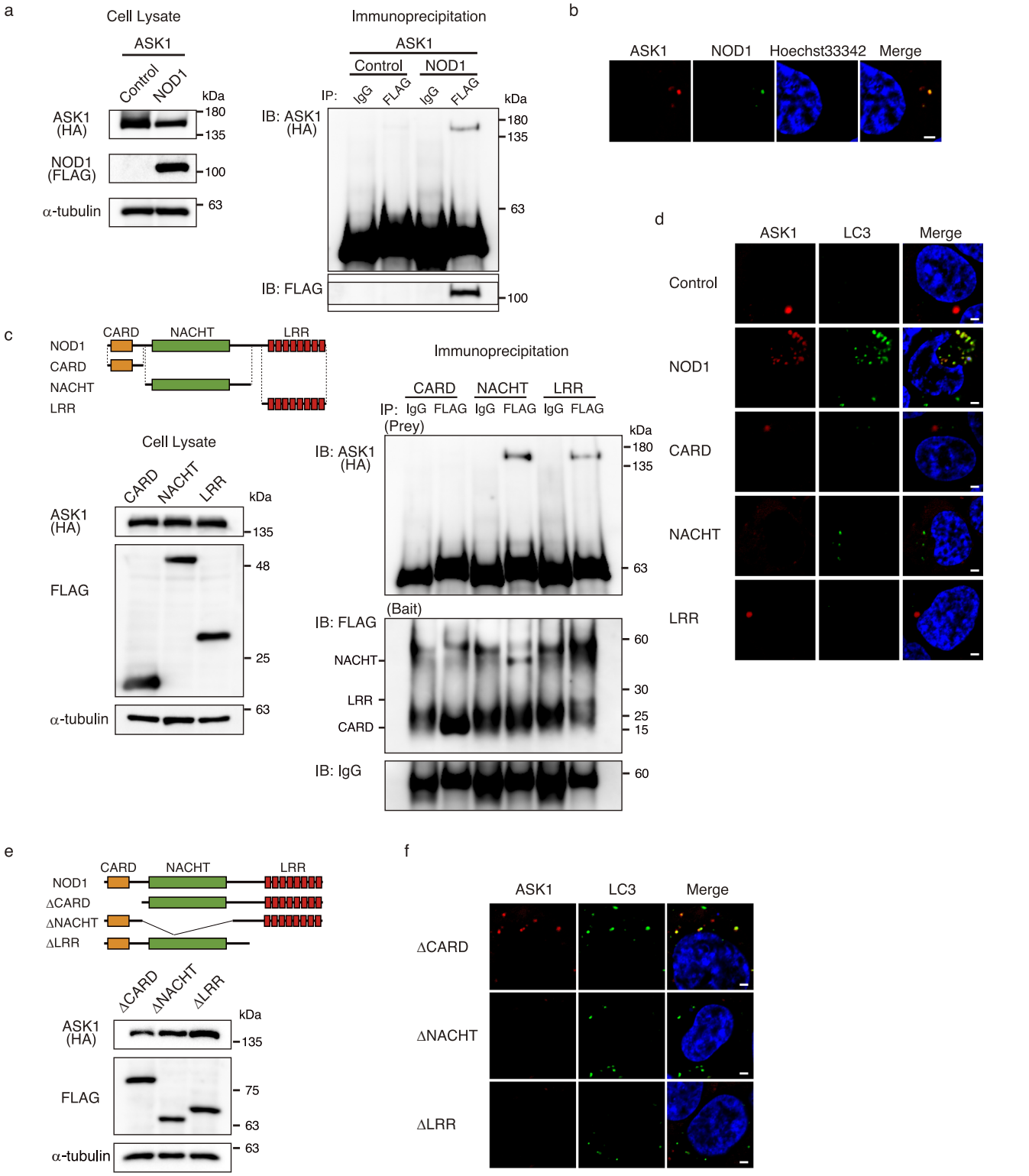

Fig. 5 | NOD1 interacts directly with ASK1. a HEK293T cells were transfected with HA-ASK1 or FLAG-NOD1. (Left) Immunoblotting of the cell lysate. (Right) Immunoprecipitation with mouse anti-FLAG antibody or control mouse IgG. **b** EGFP-NOD1 (green) transfected into stable mCherry-ASK1 (red) cells. Bars represent 2 μm. **c** HEK293T cells overexpressing HA-ASK1 transfected with FLAG-CARD, FLAG-NACHT, or FLAG-LRR domains. (Left) Immunoblotting of the cell lysate. (Right) Immunoprecipitation using mouse anti-FLAG antibody or control mouse IgG. (Right Upper) Immunoblot with mouse anti-HA antibody (prey proteins). (Right Middle) Immunoblot with rabbit anti-FLAG antibody (bait proteins). (Right Lower) The control mouse IgG blot for bait proteins. **d** Each domain of NOD1 transfected into stable mCherry-ASK1 (red) and EGFP-LC3 (green) cells. Bars represent 2 μm. **e**, **f** The deleted form of each NOD1 domain transfected into (**e**) ASK1-overexpressing HEK293T cells or (**f**) stable mCherry-ASK1 and EGFP-LC3 cell lines. **b**, **d**, and **f** Nuclei stained with Hoechst33342. Bars represent 2 μm. IP immunoprecipitation, IB immunoblotting, HA hemagglutinin.

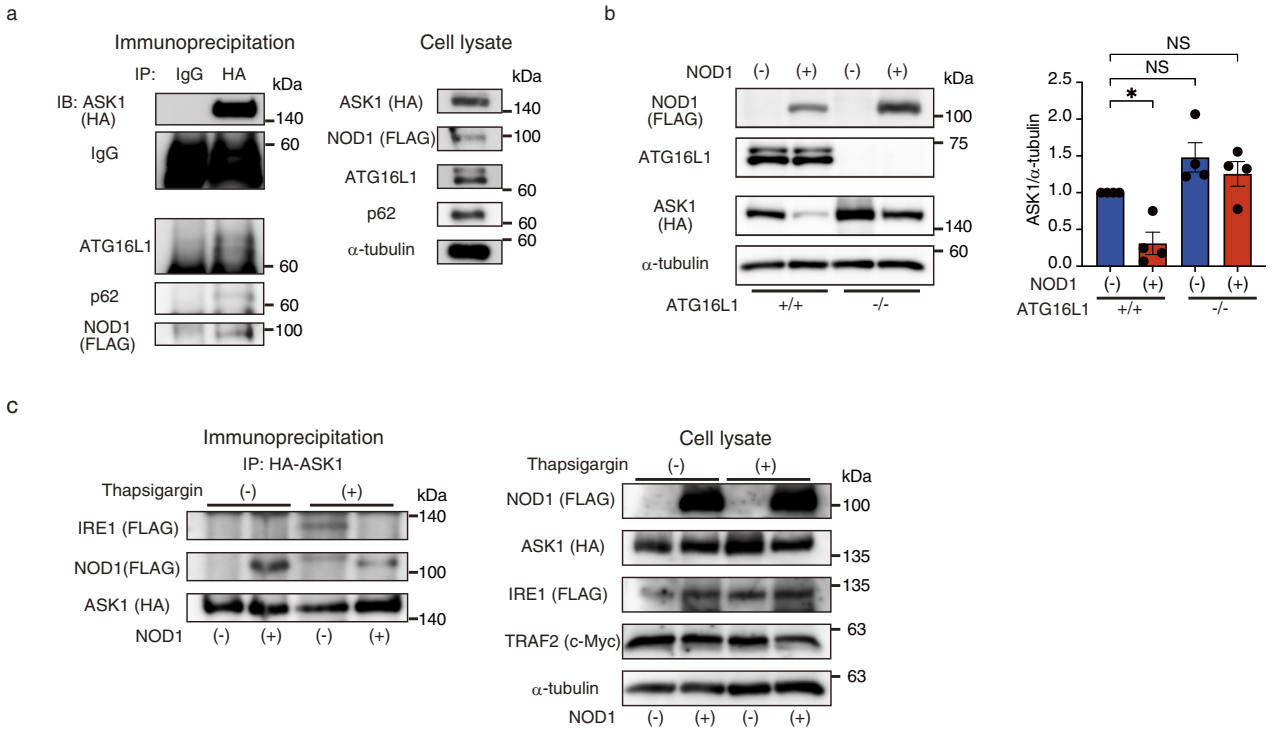

Fig. 6 | NOD1 induces ATG16L1-dependent autophagy in ASK1 and inhibits its complex formation with IRE1α. a HEK293T cells were transfected with HA-ASK1 and FLAG-NOD1. (Left) Immunoprecipitation with anti-HA antibody or control IgG. (Right) Immunoblotting of the cell lysate. **b** HA-ASK1 and FLAG-NOD1 were transfected into wild-type and ATG16L1 knockout cells. Repeated measures one-way ANOVA test with Dunnett's test; $*p < 0.05$, NS $p > 0.05$. $n = 4$. Data represent mean ± SEM. **c** Effect of NOD1 on the formation of ASK1-TRAF2-IRE1α complexes. ASK1, IRE1α, TRAF2, and/or NOD1 transfected into ATG16L1 knockout cells. The cells were stimulated with thapsigargin. (Right) Immunoprecipitation with anti-HA antibody. (Left) Immunoblotting of the cell lysate. IP immunoprecipitation, IB immunoblotting, HA hemagglutinin, NS not significant.

The exacerbation of inflammation in NOD1-KO mice with CAWS-induced coronary arteritis was dependent on ASK1, which reportedly induces the activation of p38 MAPK and c-Jun N-terminal kinase[54]. ASK1 is expressed in most organs and is activated in response to cellular stresses, such as oxidative stress[55], ER stress[46], and calcium signaling[56]. The activation of ASK1 in response to these stresses induces inflammation and cell death[57]. Excessive or prolonged activation of ASK1 in response to stress is involved in inflammatory pathogenesis. Further, ASK1 deficiency can relieve chronic renal, hepatic, and neurological disorders[57]. ASK1 suppression was previously shown to alleviate arthritis[58,59]. Therefore, the proper regulation of ASK1 activity controls inflammation.

Herein, ASK1 activation due to NOD1 deficiency increased CAWS-induced NLRP3 expression and IL-1β secretion. ASK1-mediated regulation of NLRP3 expression has been reported previously. Further, ASK1 deficiency was previously reported to downregulate NLRP3 expression in macrophages, suppressing NLRP3 inflammasome activation and markedly reducing IL-1β secretion[60]. Oxidized LDL upregulates NLRP3 expression via ASK1 activation in human aortic endothelial cells[61]. Furthermore, NLRP3 and inflammatory cytokine expression were promoted by the activation of ASK1 and p38 MAPK in retinal microvascular endothelial cells exposed to high glucose[62].

In the present study, the anti-inflammatory effect of NOD1 via ASK1 regulation was examined in adherent BMDCs as $CD11c^+$ $F4/8^+$ cells were the primary IL-1β producers in the KD mouse model. However, NOD1 is expressed in non-myeloid cells including coronary endothelial cells as well as myeloid cells[3]. The activation of ASK1 contributes to endothelial cell dysfunction and death[40]. Therefore, ASK1 dysregulation in the non-myeloid cells of NOD1-KO mice may play an important role, necessitating further study.

We demonstrated that CAWS triggered ER stress, which subsequently activated ASK1. However, CAWS was previously shown to induce ROS production and promote inflammation[33]. Since ASK1 acts as a sensor for oxidative stress, ASK1-dependent IL-1β production in NOD1-KO mice may stem from both ER and oxidative stress.

Regarding the association between ER stress and NOD1, NOD1 agonist stimulation induces ER stress, with suppressed ER stress-induced inflammation in NOD1/NOD2 double-knockout mice[63]. However, this phenotype has not been reported in NOD1 single-knockout mice. Herein, ER stress-induced inflammation was not suppressed but was promoted by increased ASK1 in NOD1-KO mice. Another study showed that thapsigargin-induced ER stress was not dependent on NOD1 in human macrophages[64]. These results suggest that NOD1 plays different roles in ER stress-induced inflammation depending on the presence of NOD1 ligands: a pro-inflammatory role through receptor activation in their presence, and an anti-inflammatory role through autophagy in their absence.

Further, we demonstrated that autophagy is involved in the regulation of ASK1 by NOD1. NOD1 is associated with autophagy induced through adaptor protein RIPK2-dependent and -independent pathways. NOD1 binds to RIPK2 via its CARD domain and subsequently induces NF-κB activation[4]. In the RIPK2-dependent pathway, RIPK2 oligomers undergo p62-dependent autophagy, with NOD1 and its ligand peptidoglycan undergoing selective autophagy through their interaction with RIPK2[12,49]. Meanwhile, the RIPK2-independent pathway is mediated ATG16L1[23]. Bacteria are recognized by NOD1, and ATG16L1 is directed to the site of bacterial invasion, facilitating their incorporation into autophagosomes. This pathway is also independent of NF-κB. Herein, we show that ASK1 degradation does not involve the CARD but requires ATG16L1, suggesting that ASK1 is degraded in a RIPK2-independent manner. NOD1-associated autophagy is effective in eliminating bacteria and PAMPs. However, our findings suggest that NOD1-induced autophagy also targets specific intracellular proteins to regulate cellular function.

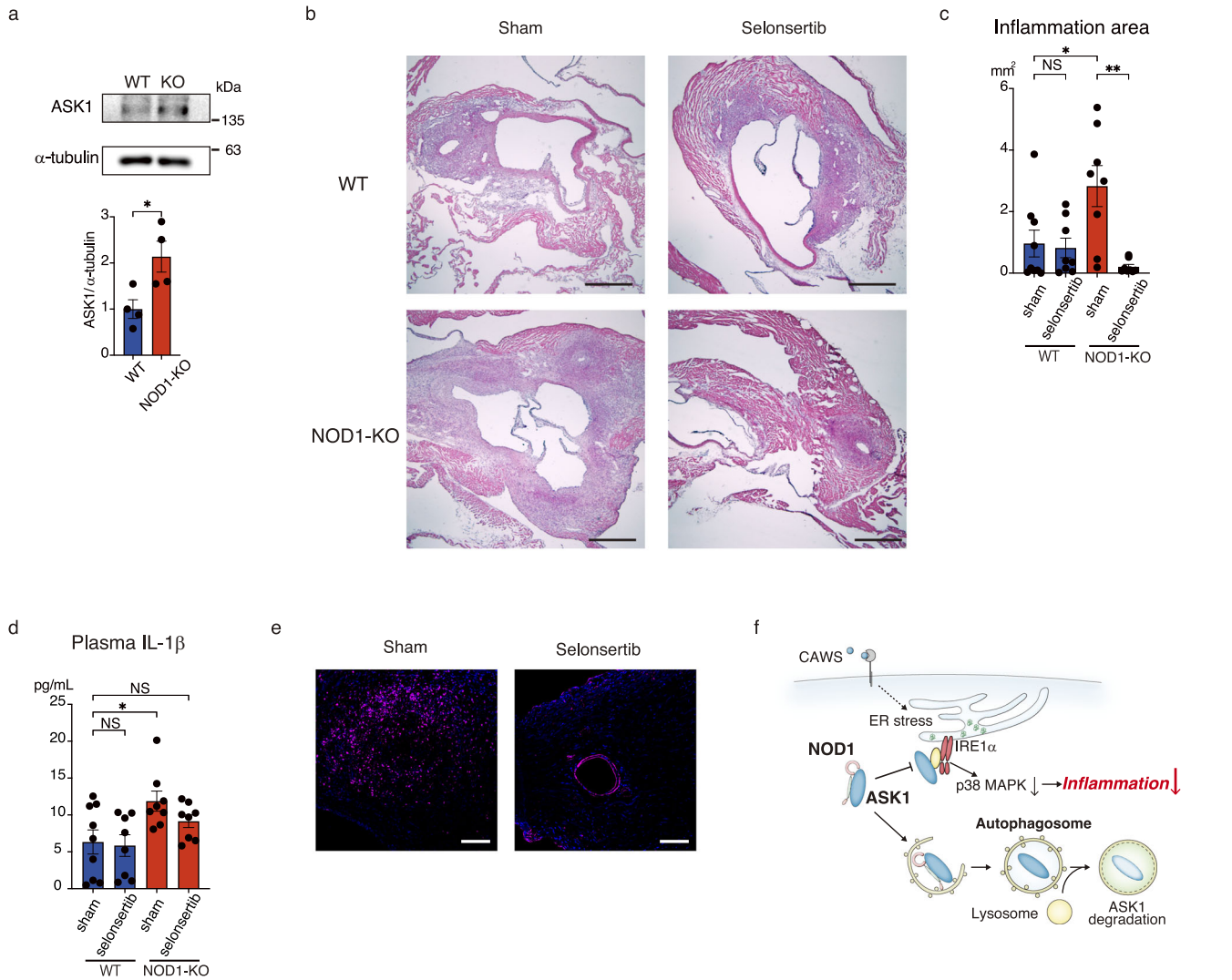

Fig. 7 | Exaggerated inflammation in CAWS-induced coronary arteritis in NOD1-KO mice is dependent on ASK1. a ASK1 levels in leukocytes from WT and NOD1-KO mice. Mann–Whitney *U* test; $^{*}p < 0.05$. $n = 4$. **b**–**e** CAWS-induced coronary arteritis in WT and NOD1-KO mice administered ASK1 inhibitor selonsertib (15 mg/kg/day) intraperitoneally once daily starting the day after consecutive CAWS injections. WT sham, $n = 9$; WT selonsertib, $n = 8$; NOD1-KO sham, $n = 8$; and NOD1-KO selonsertib, $n = 8$. **b** Hematoxylin–eosin staining in the coronary arteries and the aortic roots. Bars represent 500 μm. **c** Area of inflammatory cell infiltration in each mouse. Kruskal–Wallis test with Dunn's test; $^{*}p < 0.05$, $^{**}p < 0.01$, and NS $p > 0.05$. **d** Plasma IL-1β levels at 28 d in WT and NOD1-KO mice with CAWS-induced coronary arteritis with or without selonsertib administration, as measured via ELISA. One-way analysis of variance with the Šídák multiple comparison test; $^{*}p < 0.05$ and NS $p > 0.05$. **e** Immunofluorescence of IL-1β (magenta) and DAPI (blue) in the coronary arteries of NOD-KO mice treated with or without selonsertib. Bars represent 100 μm. **f** NOD1 suppresses the ASK1-dependent inflammatory pathway. Data represent mean ± SEM. WT wild-type, NOD1-KO NOD1-deficient, CAWS *Candida albicans* water-soluble fraction, NS not significant.

ATG16L1 forms a complex with ATG5 and ATG12, which localizes to the phagophore and facilitates LC3 lipidation and autophagosome formation[48,65]. p62 is a major cargo receptor in mammals. In selective autophagy, specific autophagic cargos are tagged with ubiquitin, leading to the assembly of adaptor proteins such as p62, NBR1, and OPTN. p62 binds to LC3 and delivers cargo to phagophores[47]. ATG16L1 and p62 cooperate in autophagy. During autophagy, p62 and ubiquitinated substrates gather with ATG9 and ATG16L1, subsequently forming autophagosomes[66]. Furthermore, ATG16L1 and p62 interactions are responsible for the formation of LC3-associated phagosomes including pathogens, in the early stage of xenophagy against *Streptococcus pneumoniae*[67]. The coordination between ATG16L1 and p62 may be involved in the autophagic degradation of ASK1 induced by NOD1. However, the detailed mechanism of ASK1 autophagic degradation warrants further investigation.

In conclusion, CAWS-induced coronary arteritis and inflammatory cytokine expression are exacerbated in NOD1-KO mice in an ASK1-dependent manner. Further, CAWS stimulation triggers ER stress, with NOD1 acting in an anti-inflammatory manner in response to ER stress-induced inflammation by suppressing ASK1–MAPK signaling. In addition, NOD1 binding to ASK1 induces ASK1 autophagy and competitively inhibits IRE1α–TRAF2–ASK1 complex formation. Altogether, these results indicate a novel role for NOD1 in autophagy substrate selectivity, suggesting that NOD1 helps maintain homeostasis in response to stress (Fig. 7f). The current findings provide novel insights into the underlying mechanisms that link inflammation and autophagy.

Methods

Ethics approval

All animal experiments were performed in accordance with institutional regulations and compliance with the Act on Welfare and Management of Animals and related guidelines in Japan. The experimental procedures were approved by the animal experimentation ethics and genetically modified

organism experimental safety committees of Teikyo University School of Medicine, Tokyo, Japan – approval: 16-008, 23-012, 2002209B3b, 2303386A1b. We have complied with all relevant ethical regulations for animal use. In addition, all experimental procedures were executed in alignment with the ARRIVE guidelines, ensuring strict observance of humane endpoints and animal welfare principles throughout the research process.

Mice

Mice were housed in a temperature-controlled environment with a 12-h light/dark cycle at the Central Experimental Animal Center, Teikyo University School of Medicine (Tokyo, Japan). WT C57BL/6 mice were purchased from Sankyo Labo Service Corporation (Tokyo, Japan). Homozygous NOD1-KO C57BL/6 mice were kindly provided by Prof. T. Hara (Kyushu University, Fukuoka, Japan) and have been previously described[4,68]. Homozygous IL-1R1-KO C57BL/6 mice were purchased from the Jackson Laboratory (ME, USA) and have been previously described[69]. NOD1-KO and IL-1R1-KO mice were crossed, and F1 mice were crossed and created NOD1/IL-1R1-DKO mice. Tail snips were obtained from the mice and used for genotyping through polymerase chain reaction (PCR) analysis using primers specific for the WT, mutant-type NOD1 alleles, and mutant-type IL-1R1 alleles. Primers used for genotyping are listed in Supplementary Table 3. In all experiments, mice were euthanized using isoflurane (Wako, Tokyo, Japan). The individual mouse is the experimental unit. No mice were excluded from the analysis.

CAWS-induced coronary arteritis mouse model

CAWS was prepared from *Candida albicans* strain NBRC1385, as previously described[29]. Next, it was used to induce vasculitis, as previously described[27]. Sex-matched female or male mice (aged 5–7 weeks) were used in all experiments.

Herein, 0.2 mL of 10 mg/mL CAWS solution dissolved in phosphate-buffered saline (PBS) was injected intraperitoneally into WT, NOD1-KO, and NOD1/IL-1R1-DKO mice on five consecutive days. At 28 d after CAWS injection, the mice were sacrificed.

The ASK1 inhibitor selonsertib (MedChemExpress, NJ, USA) was dissolved at a concentration of 1.5 mg/mL in 10% dimethyl sulfoxide, 40% polyethylene glycol 300, 5% Tween 80, and normal saline. WT and NOD1-KO mice were randomly divided into two groups each, receiving either selonsertib solution (200 µL, 15 mg/kg/d) or solvent intraperitoneally once daily from the day after consecutive injections of CAWS to the day before sacrifice.

Histological evaluation

The hearts of mice were fixed with 4% paraformaldehyde, and serially frozen sections of the coronary arteries and aortic roots were stained with hematoxylin and eosin before being imaged using a BX53 microscope (Olympus, Hachioji, Japan). Lesion assessment was performed as previously described[70]. Lesions were assessed in the following five segments: left and right coronary arteries, left and right coronary sinuses, and non-coronary sinus. The degree of inflammation in each segment was assessed as follows: 0, no inflammation; 1, inflammation in the intima (namely endarteritis); 2, inflammation in the intima and adventitia; and 3, inflammation in all layers of the vascular wall (namely panvasculitis). The rate of panvasculitis was defined as the percentage of mice which presented one or more panvasculitis lesions. The severity score was defined as the average inflammatory score per segment, and the number of lesions was defined as the total number of segments with an inflammatory score of ≥1. The inflammation area was defined as the largest area of inflammatory cell infiltration among the serially frozen sections of each mouse.

Culturing adherent BMDCs

BMDCs were isolated as previously described[71]. The BM was isolated by flushing the tibiae and femora with cold PBS. BM cells (5×10^6 cells) were cultured and differentiated into BMDCs in 100-mm dishes in 10 mL of complete medium (Roswell Park Memorial Institute Medium [RPMI] 1640 supplemented with 10% heat-inactivated FBS, 2 mmol/L L-glutamine, 100 U/mL penicillin, 100 µg/mL streptomycin, 50 µmol/L 2-mercaptomethanol, and 20 ng/mL murine granulocyte macrophage colony-stimulating factor [Peprotech, NJ, USA]). The complete medium (5 mL) was added on day 3, and 5 mL of the medium was replaced with an equal volume of fresh medium on day 6. On day 8, non-adherent cells were discarded, and adherent cells were detached using trypsin and suspended at a concentration of 1×10^6 cells/mL in the complete medium. Then, 100, 200, 500, and 1000 µL of the cell suspension was seeded in 96-, 48-, 24-, and 12-well plates, respectively. After approximately 36 h of culture, cells were used for further experiments.

RNA-seq

The samples were treated with the TRIZOL reagent (Thermo Fisher Scientific, MA, USA). Purified total RNA was resuspended in H_2O, and the total RNA was quantified using a Nanodrop spectrophotometer (Thermo Fisher Scientific, MA, USA) and RNA 6000 Pico Kit (Agilent Technologies, CA, USA) for RNA quality control (QC). Total RNA (500 ng of the quantified RNA) was used for ribosomal RNA (rRNA) depletion using the rRNA-depletion kit (New England Biolabs, MA, USA), followed by directional library synthesis using the NEB Next Ultra Directional RNA Library Prep Kit (New England Biolabs, MA, USA). Library QC was performed using the Agilent Bioanalyzer DNA High-Sensitivity Kit (Agilent Technologies, CA, USA). Sequencing was performed using NextSeq500 (Illumina, Inc., CA, USA) with a high-output kit in paired-end reads (v2, 2 × 36). The FASTQ files were imported into the CLC Genomics Workbench (CLC GW, v10.1.1, Qiagen, Venlo, Netherlands). Sequence reads were mapped to the mouse reference genome (mm10) and qualified for 49,575 genes. The procedure was performed in Tsukuba i-Laboratory LLP (Tsukuba, Ibaraki, Japan).

DEGs (false discovery rate [FDR] q-value ≤ 0.05, fold change ≥ 2.0) were detected using the CLC Main Workbench Gaussian-based test. For enrichment analysis, Gene Ontology (GO) terms enriched in DEGs were identified using the Database for Annotation, Visualization, and Integrated Discovery (DAVID) (https://david.ncifcrf.gov/tools.jsp). GSEA was performed to identify the biological pathways differentially enriched between BMDCs from CAWS-stimulated WT and NOD1-KO mice using the GSEA software (Broad Institute, MA, USA). The variable genes common to CAWS stimulation were extracted as genes in common with genes whose expression varied before and after CAWS stimulation in WT and NOD1-KO cells (FDR q-value ≤ 0.05, maximum fold change ≥ 2.0). The ER stress-related genes were searched among the DEGs (1782 genes), and their enrichment was analyzed using a membership search of the gene list analysis in the Metascape (https://metascape.org/). In total, 68 genes were extracted. A heatmap of ER stress-related genes was generated using Morpheus (https://software.broadinstitute.org/morpheus/). The hierarchical clustering of the 68 genes was based on 1-Pearson correlation. Enrichment analysis was performed for 68 genes using DAVID and GO.

mCherry-ASK1 and/or EGFP-LC3B stable expression cell line

The expression vector of mCherry-ASK1 was transfected into HEK 293 T cells using the ViaFect Transfection reagent. At 24 h after transfection, 200 µg/mL hygromycin (Wako, Tokyo, Japan) was added to select transformants. Surviving cells were seeded in 96-well plates via single-cell plating. The stable expression of mCherry-ASK1 was validated through fluorescence microscopy, real-time reverse transcriptase PCR (RT-PCR), and western blotting. Next, the expression vector of EGFP-LC3B was transfected into mCherry-ASK1 stable cells. Cells were selected using 1 µg/mL puromycin (Wako, Tokyo, Japan). The method for obtaining individual clones was the same as described above.

Knockout of ATG16L1

ATG16L1 was knocked out using the CRISPR-Cas9 system. Single guide RNA (sgRNA) sequences for ATG16L1 knockout were obtained from a previous study (Supplementary Table 3)[72]. The plasmid vector, namely pGedit, expressed Cas9 protein, sgRNAs, and

a fusion protein of EGFP and blastcidin S deaminase as selection markers. pGedit (RDB16763) was obtained from RIKEN BRC (Tsukuba, Ibaraki, Japan), and the detailed method has been described previously[73]. The sgRNA sequence was inserted downstream of the U6 promoter in pGedit using the NEBridge Golden Gate Assembly Kit (BsmBI-v2) (New England Biolabs, MA, USA). The vector was transfected into HEK293T cells using the ViaFect Transfection Reagent (Promega, WI, USA). At 24 h after transfection, 50 μg/mL blastcidin S (Wako, Tokyo, Japan) was added to the cultures to select the transformants. The medium was changed to remove blastcidin S after 48-h incubation. After 2 d, the cells were seeded in a 100-mm dish. Non-fluorescent colonies were selected to exclude Cas9-stable expression cells and were cultured in 48-well plates. To examine the ATG16L1 homozygous knockout clone, a T7 endonuclease I-based mutation detection assay was performed using a Rapid Indel Detection Kit (Nippon Gene Co., Tokyo, Japan). DNA sequencing was performed by Eurofins Genomics K.K. (Tokyo, Japan). The deletion of ATG16L1 was validated using RT-PCR and western blotting.

Statistics and reproducibility

All data are expressed as mean ± standard error of the mean. All experiments were repeated at least three times. The assumption of normality of data was tested using the Shapiro–Wilk normality test. If normality was rejected, the results were further analyzed using the Mann–Whitney *U* test (for two groups) or the Kruskal–Wallis test, followed by Dunn's post hoc test (for more than two groups). If normality was not rejected, the *F*-test or Brown–Forsythe test was used to evaluate the equality of variance. If the variance among groups was assumed to be equal, an unpaired *t*-test (in two groups) or an ordinary one-way analysis of variance (ANOVA), followed by the Šídák post hoc test (in more than two groups) was performed. If the variance was not assumed equal, an unpaired *t*-test with Welch's correction (in two groups) or the Brown–Forsythe and Welch's ANOVA test, followed by Dunnett's post hoc test (in more than two groups) was performed. A ratio-paired *t*-test was used to compare the ratios against controls. Differences were considered statistically significant at $p < 0.05$. All analyses were performed using the GraphPad Prism 9 software (GraphPad Software, CA, USA).

For further information, please see Supplementary Methods.

Reporting summary

Further information on research design is available in the Nature Portfolio Reporting Summary linked to this article.

Data availability

RNA-seq data that support the findings of this study have been deposited in NCBI GEO with the accession code: GSE278589. Data used for Figures and Supplementary Figures are provided in Supplementary Datas 1 and 2. All uncropped blot images are included in the Supplementary information. The data that support the findings of this study are available from the corresponding author, Yoshitaka Kimura, upon reasonable request.

Received: 3 October 2024; Accepted: 13 May 2025;
Published online: 21 May 2025

References

1. Jones, J. D. G., Vance, R. E. & Dangl, J. L. Intracellular innate immune surveillance devices in plants and animals. *Science* **354**, aaf6395 (2016).
2. Boyle, J. P., Mayle, S., Parkhouse, R. & Monie, T. P. Comparative genomic and sequence analysis provides insight into the molecular functionality of NOD1 and NOD2. *Front. Immunol.* **4**, 63978 (2013).
3. Moreira, L. O. & Zamboni, D. S. NOD1 and NOD2 signaling in infection and inflammation. *Front. Immunol.* **3**, 328 (2012).
4. Chamaillard, M. et al. An essential role for NOD1 in host recognition of bacterial peptidoglycan containing diaminopimelic acid. *Nat. Immunol.* **4**, 702–707 (2003).
5. Maisonneuve, C. et al. Nod1 promotes colorectal carcinogenesis by regulating the immunosuppressive functions of tumor-infiltrating myeloid cells. *Cell Rep.* **34**, 108677 (2021).
6. Joosten, L. A. B. et al. Differential function of the NACHT-LRR (NLR) members Nod1 and Nod2 in arthritis. *Proc. Natl. Acad. Sci. USA* **105**, 9017–9022 (2008).
7. Chen, G. Y., Shaw, M. H., Redondo, G. & Núñez, G. The innate immune receptor Nod1 protects the intestine from inflammation-induced tumorigenesis. *Cancer Res.* **68**, 10060–10067 (2008).
8. Deretic, V. Autophagy in inflammation, infection, and immunometabolism. *Immunity* **54**, 437 (2021).
9. Levine, B. Eating oneself and uninvited guests: autophagy-related pathways in cellular defense. *Cell* **120**, 159–162 (2005).
10. Gutierrez, M. G. et al. Autophagy is a defense mechanism inhibiting BCG and Mycobacterium tuberculosis survival in infected macrophages. *Cell* **119**, 753–766 (2004).
11. Nakagawa, I. et al. Autophagy defends cells against invading group A Streptococcus. *Science* **306**, 1037–1040 (2004).
12. Irving, A. T. et al. The immune receptor NOD1 and kinase RIP2 interact with bacterial peptidoglycan on early endosomes to promote autophagy and inflammatory signaling. *Cell Host Microbe* **15**, 623–635 (2014).
13. Nakahira, K. et al. Autophagy proteins regulate innate immune responses by inhibiting the release of mitochondrial DNA mediated by the NALP3 inflammasome. *Nat. Immunol.* **12**, 222–230 (2011).
14. Maejima, I. et al. Autophagy sequesters damaged lysosomes to control lysosomal biogenesis and kidney injury. *EMBO J.* **32**, 2336 (2013).
15. Mehto, S. et al. The Crohn's disease risk factor IRGM limits NLRP3 inflammasome activation by impeding its assembly and by mediating its selective autophagy. *Mol. Cell* **73**, 429–445.e7 (2019).
16. Shi, C. S. et al. Activation of autophagy by inflammatory signals limits IL-1β production by targeting ubiquitinated inflammasomes for destruction. *Nat. Immunol.* **13**, 255–263 (2012).
17. Jena, K. K. et al. Autoimmunity gene IRGM suppresses cGAS-STING and RIG-I-MAVS signaling to control interferon response. *EMBO Rep.* **21**, e50051 (2020).
18. Clarke, A. J. et al. Autophagy is activated in systemic lupus erythematosus and required for plasmablast development. *Ann. Rheum. Dis.* **74**, 912–920 (2015).
19. Gonzalez, C. D. et al. The emerging role of autophagy in the pathophysiology of diabetes mellitus. *Autophagy* **7**, 2–11 (2011).
20. Razani, B. et al. Autophagy links inflammasomes to atherosclerotic progression. *Cell Metab.* **15**, 534–544 (2012).
21. Lynch-Day, M. A., Mao, K., Wang, K., Zhao, M. & Klionsky, D. J. The role of autophagy in Parkinson's disease. *Cold Spring Harb. Perspect. Med.* **2**, a009357–a009357 (2012).
22. Hayrabedyan, S. et al. Sertoli cells have a functional NALP3 inflammasome that can modulate autophagy and cytokine production. *Sci. Rep.* **6**, 1–17 (2016).
23. Travassos, L. H. et al. Nod1 and Nod2 direct autophagy by recruiting ATG16L1 to the plasma membrane at the site of bacterial entry. *Nat. Immunol.* **11**, 55–62 (2009).
24. Nishio, H. et al. Nod1 ligands induce site-specific vascular inflammation. *Arterioscler Thromb. Vasc. Biol.* **31**, 1093–1099 (2011).
25. Onoyama, S. et al. Genetic susceptibility to Kawasaki disease: analysis of pattern recognition receptor genes. *Hum. Immunol.* **73**, 654–660 (2012).
26. Kusuda, T. et al. Kawasaki disease-specific molecules in the sera are linked to microbe-associated molecular patterns in the biofilms. *PLoS ONE* **9**, e113054 (2014).

27. Takahashi, K. et al. Histopathological features of murine systemic vasculitis caused by Candida albicans extract - An animal model of Kawasaki Disease. *Inflamm. Res.* **53**, 72–77 (2004).
28. Doung, T. T., Silverman, E. D., Bissessar, M. V. & Yeung, R. S. M. Superantigenic activity is responsible for induction of coronary arteritis in mice: an animal model of Kawasaki disease. *Int Immunol.* **15**, 79–89 (2003).
29. Saijo, S. et al. Dectin-2 recognition of α-Mannans and induction of Th17 cell differentiation is essential for host defense against candida albicans. *Immunity* **32**, 681–691 (2010).
30. Miyabe, C. et al. Dectin-2–induced CCL2 production in tissue-resident macrophages ignites cardiac arteritis. *J. Clin. Invest.* **129**, 3610–3624 (2019).
31. Hashimoto, Y. et al. Interleukin-1beta inhibition attenuates vasculitis in a mouse model of Kawasaki disease. *J. Nippon Med. Sch.* **86**, 108–116 (2019).
32. Lee, Y. et al. Interleukin-1β is crucial for the induction of coronary artery inflammation in a mouse model of kawasaki disease. *Circulation* **125**, 1542–1550 (2012).
33. Anzai, F. et al. Crucial role of NLRP3 inflammasome in a murine model of Kawasaki disease. *J. Mol. Cell Cardiol.* **138**, 185–196 (2020).
34. Lee, Y. et al. IL-1 signaling is critically required in stromal cells in Kawasaki disease vasculitis mouse model. Role of both IL-1α and IL-1β HHS public access. *Arterioscler Thromb. Vasc. Biol.* **35**, 2605–2616 (2015).
35. Wang, J. et al. Discrimination of the heterogeneity of bone marrow-derived dendritic cells. *Mol. Med. Rep.* **16**, 6787–6793 (2017).
36. Wan, P. et al. Extracellular ATP mediates inflammatory responses in colitis via P2X7 receptor signaling. *Sci. Rep.* **6**, 1–10 (2016).
37. Riteau, N. et al. Extracellular ATP is a danger signal activating P2X7 receptor in lung inflammation and fibrosis. *Am. J. Respir. Crit. Care Med.* **182**, 774–783 (2010).
38. Iwata, M. et al. Psychological stress activates the inflammasome via release of adenosine triphosphate and stimulation of the purinergic type 2X7 receptor. *Biol. Psychiatry* **80**, 12–22 (2016).
39. Carta, S. et al. Cell stress increases ATP release in NLRP3 inflammasome-mediated autoinflammatory diseases, resulting in cytokine imbalance. *Proc. Natl. Acad. Sci. USA* **112**, 2835–2840 (2015).
40. Jia, C. et al. Endothelial cell pyroptosis plays an important role in Kawasaki disease via HMGB1/RAGE/cathespin B signaling pathway and NLRP3 inflammasome activation. *Cell Death Dis.* **10**, 1–16 (2019).
41. Zhang, D., Liu, L., Huang, X. & Tian, J. Insights into coronary artery lesions in Kawasaki disease. *Front. Pediatr.* **8**, 493 (2020).
42. Robinson, M. J. et al. Dectin-2 is a Syk-coupled pattern recognition receptor crucial for Th17 responses to fungal infection. *J. Exp. Med.* **206**, 2037 (2009).
43. Grootjans, J., Kaser, A., Kaufman, R. J. & Blumberg, R. S. The unfolded protein response in immunity and inflammation. *Nat. Rev. Immunol.* **16**, 469 (2016).
44. Marek-Iannucci, S. et al. Targeting IRE1 endoribonuclease activity alleviates cardiovascular lesions in a murine model of Kawasaki disease vasculitis. *JCI Insight* **7**, e157203 (2022).
45. Sasaki, I. et al. A stress sensor, IRE1α, is required for bacterial-exotoxin-induced interleukin-1β production in tissue-resident macrophages. *Cell Rep.* **43**, 113981 (2024).
46. Nishitoh, H. et al. ASK1 is essential for endoplasmic reticulum stress-induced neuronal cell death triggered by expanded polyglutamine repeats. *Genes Dev.* **16**, 1345 (2002).
47. Gubas, A. & Dikic, I. A guide to the regulation of selective autophagy receptors. *FEBS J.* **289**, 75–89 (2022).
48. Gammoh, N. The multifaceted functions of ATG16L1 in autophagy and related processes. *J. Cell Sci.* **133**, jcs249227 (2020).
49. Mehto, S. et al. Selective autophagy of RIPosomes maintains innate immune homeostasis during bacterial infection. *EMBO J.* **41**, e111289 (2022).
50. Rosenkranz, M. E. et al. TLR2 and MyD88 contribute to Lactobacillus casei extract-induced focal coronary arteritis in a mouse model of Kawasaki disease. *Circulation* **112**, 2966–2973 (2005).
51. Fujieda, Y. et al. Inflammation and resolution are associated with upregulation of fatty acid β-Oxidation in Zymosan-Induced Peritonitis. *PLoS ONE* **8**, e66270 (2013).
52. Mariotte, A. et al. A mouse model of MSU-induced acute inflammation in vivo suggests imiquimod-dependent targeting of *Il-1β* as relevant therapy for gout patients. *Theranostics* **10**, 2158–2171 (2020).
53. Marinho, Y. et al. MSU Crystals induce sterile IL-1β secretion via P2X7 receptor activation and HMGB1 release. *Biochim. Biophys. Acta Gen. Subj.* **1864**, 129461 (2020).
54. Ichijo, H. et al. Induction of apoptosis by ASK1, a mammalian MAPKKK that activates SAPK/JNK and p38 signaling pathways. *Science* **275**, 90–94 (1997).
55. Fujino, G. et al. Thioredoxin and TRAF family proteins regulate reactive oxygen species-dependent activation of ASK1 through reciprocal modulation of the N-terminal homophilic interaction of ASK1. *Mol. Cell Biol.* **27**, 8152–8163 (2007).
56. Samak, G. et al. Calcium/Ask1/MKK7/JNK2/c-Src signalling cascade mediates disruption of intestinal epithelial tight junctions by dextran sulfate sodium. *Biochem J.* **465**, 503–515 (2015).
57. Ogier, J. M., Nayagam, B. A. & Lockhart, P. J. ASK1 inhibition: a therapeutic strategy with multi-system benefits. *J. Mol. Med (Berl.)* **98**, 335–348 (2020).
58. Mnich, S. J. et al. Critical role for apoptosis signal-regulating kinase 1 in the development of inflammatory K/BxN serum-induced arthritis. *Int Immunopharmacol.* **10**, 1170–1176 (2010).
59. Nygaard, G. et al. Regulation and function of apoptosis signal-regulating kinase 1 in rheumatoid arthritis. *Biochem Pharm.* **151**, 282–290 (2018).
60. Immanuel, C. N. et al. Apoptosis signal-regulating kinase-1 promotes inflammasome priming in macrophages. *Am. J. Physiol. Lung Cell Mol. Physiol.* **316**, L418–L427 (2019).
61. Hang, L., Peng, Y., Xiang, R., Li, X. & Li, Z. Ox-LDL causes endothelial cell injury through ASK1/NLRP3-mediated inflammasome activation via endoplasmic reticulum stress. *Drug Des. Devel. Ther.* **14**, 731 (2020).
62. Zou, W. et al. ASK1/p38-mediated NLRP3 inflammasome signaling pathway contributes to aberrant retinal angiogenesis in diabetic retinopathy. *Int. J. Mol. Med.* **47**, 732–740 (2021).
63. Keestra-Gounder, A. M. et al. NOD1 and NOD2 signalling links ER stress with inflammation. *Nature* **532**, 394–397 (2016).
64. Huang, C., Hedl, M., Ranjan, K. & Abraham, C. LACC1 required for NOD2-induced, ER stress-mediated innate immune outcomes in human macrophages and LACC1 risk variants modulate these outcomes. *Cell Rep.* **29**, 4525 (2019).
65. Dudley, L. J. et al. Intrinsic lipid binding activity of ATG 16L1 supports efficient membrane anchoring and autophagy. *EMBO J.* **38**, e100554 (2019).
66. Feng, X. et al. Local membrane source gathering by p62 body drives autophagosome formation. *Nat. Commun.* **14**, 1–14 (2023).
67. Ogawa, M. et al. Streptococcus pneumoniae triggers hierarchical autophagy through reprogramming of LAPosome-like vesicles via NDP52-delocalization. *Commun. Biol.* **3**, 1–15 (2020).
68. Inoue, H. et al. Activation of Nod1 signaling induces fetal growth restriction and death through fetal and maternal vasculopathy. *J. Immunol.* **196**, 2779–2787 (2016).
69. Glaccum, M. B. et al. Phenotypic and functional characterization of mice that lack the type I receptor for IL-I. *J. Immunol.* **159**, 3364–3371 (1997).

70. Takahashi, K. et al. Administration of human immunoglobulin suppresses development of murine systemic vasculitis induced with Candida albicans water-soluble fraction: an animal model of Kawasaki disease. *Mod. Rheumatol.* **20**, 160–167 (2010).
71. Sauter, M. et al. Protocol to isolate and analyze mouse bone marrow derived dendritic cells (BMDC). *STAR Protoc.* **3**, 101664 (2022).
72. Ulferts, R. et al. Subtractive CRISPR screen identifies the ATG16L1/vacuolar ATPase axis as required for non-canonical LC3 lipidation. *Cell Rep.* **37**, 109899 (2021).
73. Nagasaki, A. et al. A genome editing vector that enables easy selection and identification of knockout cells. *Plasmid* **98**, 37–44 (2018).

Acknowledgements

Y.K. was supported by JSPS KAKENHI Grant Number JP21K16217. H.K. was supported by JSPS KAKENHI Grant Number JP21K08480.

Author contributions

Y.K.: Conceptualization, Data curation, Formal Analysis, Funding acquisition, Investigation, Project administration, Supervision, Visualization, Writing–original draft, Writing–review & editing, M.K.: Data curation, Formal Analysis, Investigation, Validation, Visualization, N.M.: Resources, Supervision, Y.Y.: Conceptualization, Formal Analysis, Validation, Writing–review & editing, H.K.: Conceptualization, Formal Analysis, Funding acquisition, Project administration, Supervision, Writing–review & editing.

Competing interests

The authors declare no competing interests.

Additional information

Supplementary information The online version contains supplementary material available at https://doi.org/10.1038/s42003-025-08213-6.

Correspondence and requests for materials should be addressed to Yoshitaka Kimura.

Peer review information *Communications Biology* thanks Ming-Yue Wu and the other, anonymous, reviewers for their contribution to the peer review of this work. Primary Handling Editors: Eirini Trompouki and Mengtan Xing. A peer review file is available.

Reprints and permissions information is available at http://www.nature.com/reprints

Publisher's note Springer Nature remains neutral with regard to jurisdictional claims in published maps and institutional affiliations.

Open Access This article is licensed under a Creative Commons Attribution-NonCommercial-NoDerivatives 4.0 International License, which permits any non-commercial use, sharing, distribution and reproduction in any medium or format, as long as you give appropriate credit to the original author(s) and the source, provide a link to the Creative Commons licence, and indicate if you modified the licensed material. You do not have permission under this licence to share adapted material derived from this article or parts of it. The images or other third party material in this article are included in the article's Creative Commons licence, unless indicated otherwise in a credit line to the material. If material is not included in the article's Creative Commons licence and your intended use is not permitted by statutory regulation or exceeds the permitted use, you will need to obtain permission directly from the copyright holder. To view a copy of this licence, visit http://creativecommons.org/licenses/by-nc-nd/4.0/.

© The Author(s) 2025